Available online at www.sciencedirect.com
SCIENCE DIRECT
Journal of Magnetic Resonance 180 (2006) 236–244
JMR Journal of Magnetic Resonance
www.elsevier.com/locate/jmr

Characterization of microporous aluminophosphate IST-1 using ^{1}H Lee–Goldburg techniques

Luís Mafra [a,b], João Rocha [a,*], Christian Fernandez [b], Filipe A. Almeida Paz [a]

[a] Department of Chemistry, University of Aveiro, CICECO, 3810-193 Aveiro, Portugal
[b] Laboratoire Catalyse et Spectrochimie (CNRS UMR 6506), ENSICAEN and Université de Caen-Basse Normandie, 14050 Caen, France

Received 27 December 2005; revised 21 February 2006
Available online 27 March 2006

Abstract

The presence of two independent methylamine species in microporous aluminophosphate IST-1 ($|(CH_3NH_2)_4(CH_3NH^+_3)_4(OH^-)_4|[Al_{12}P_{12}O_{48}]$) has been shown previously by synchrotron powder X-ray diffraction. One of these species, [N(1)–C(1)], links to a six-coordinated framework Al-atom [Al(1)], while the other methylamine [N(2)–C(2)] is protonated and hydrogen-bonded to three O-atoms [O(1), O(2) and O(12)]. We revisit the structure of IST-1 and report the complete assignment of the ^{1}H NMR spectra by combining X-ray data and high-resolution heteronuclear/homonuclear solid-state NMR techniques based on frequency-switched Lee–Goldburg homonuclear decoupling and ^{31}P–^{31}P homonuclear recoupling. Careful analysis of the 2D ^{1}H–X homonuclear correlation (X = ^{1}H) and 2D heteronuclear correlation (X = ^{13}C, ^{31}P and ^{27}Al) spectra allowed the distinction of both methylamine species and the assignment of all ^{31}P and ^{13}C resonances. For the first time at a relatively high (9.4 T) magnetic field, symmetric doublet patterns have been observed in the ^{13}C spectra, caused by the influence of the ^{14}N second-order quadrupolar interaction.

Keywords: FS-LG; 2D HETCOR MAS NMR; ^{31}P DQ; Inorganic–organic hybrids; Templates; Microporous aluminophosphates; Methylamine

1. Introduction

Since the pioneering work of Lee and co-workers [1] and Waugh and Fessenden [2], which lead to the introduction of the WHH-4 multiple pulse scheme, high-resolution NMR techniques based on homonuclear decoupling have been extensively studied, aiming at making them less sensitive to experimental imperfections and increasing the decoupling performance. Many pulse sequences have been developed to decrease or suppress the effects of the homonuclear dipolar interaction. Prominent examples are WHH-4 [2], MREV-8 [3,4], BR-24 [5], BLEW-48 and BLEW-12 [6], TREV-8 [7], MSHOT-3 [8], DUMBO-1 [9], FS-LG-2 [10,11], PMLGn [12–15], and wPMLGn [15]. The older sequences were designed for static conditions and, thus, are limited to relatively slow magic-angle spinning (MAS) [16]. Since the late 1970s, following the introduction of combined magic-angle-rotation and multiple-pulse (CRAMPS) by Gerstein et al. [17], these methods have been nearly always performed under MAS for averaging out other anisotropic interactions such as chemical-shift anisotry and heteronuclear dipolar interactions.

As a result of the continuous improvement of hardware and software in the last 15 years, a new generation of improved sequences has been proposed, including frequency-switched Lee–Goldburg (FS-LG). In general, the multipulse sequences fail at high MAS rates due to interference between the sample spinning and RF cycles. However, with the recent CRAMPS techniques (FS-LG-2, PMLGn, and others) based on off-resonance RF fields, it is possible to simultaneously manipulate the spin and spatial parts of the dipolar Hamiltonian without loss of decoupling efficiency. Sequences like FS-LG-2 have short cycle times

* Corresponding author.
E-mail address: rocha@dq.ua.pt (J. Rocha).

1090-7807/$ - see front matter © 2006 Elsevier Inc. All rights reserved.
doi:10.1016/j.jmr.2006.02.017

and, hence, may be combined successfully with moderately fast MAS (12–15 kHz) [18]. The FS-LG-2 decoupling scheme has found widespread application in multi-dimensional experiments involving proton evolution in the indirect dimension (F1).

Since the discovery of microporous aluminophosphates by Wilson et al. [19], much research has been concentrated on the synthesis of these materials, employing organic templates [20,21] (generally amines), which play a decisive role as structure-directing agents. Here, we report NMR studies of a templated aluminophosphate, IST-1 [22], containing two types of methylamine species: [N(1)–C(1)] (here denoted MA or $–NH_2$) is linked to six-coordinated Al atom, while [N(2)–C(2)] (MA^+ or $–NH_3^+$) resides in the channels and is probably protonated and hydrogen-bonded to three framework oxygen atoms [O(1), O(2), and O(12)]. An additional hydroxyl group [O(13)], bridging two Al-atoms [Al(1) and Al(3)], is also present [22].

We have used ^{1}H NMR resolution-enhancement techniques, such as two-dimensional (2D) ^{1}H–^{1}H homonuclear correlation (HOMCOR) and heteronuclear ^{1}H–X (X = ^{13}C, ^{31}P, ^{27}Al) correlation (HETCOR) MAS experiments using FS-LG decoupling, to elucidate the fine details of the IST-1 structure, particularly in what concerns the methyl-ammonium cations, MA^+, and Al-coordinated methylamine molecules, MA. Moreover, the ^{31}P–^{31}P double quantum (DQ)-single quantum (SQ) experiment was used to confirm the previous assignment of the IST-1 ^{31}P resonances [22]. This work is part of a comprehensive study aimed at evaluating the usefulness of high-resolution ^{1}H NMR techniques to elucidate the structure of inorganic–organic hybrid materials.

1.1. FS-LG-2 principle

The FS-LG-2 is a phase and frequency-switched technique, also called flip-flop Lee–Goldburg (FFLG) sequence. Lee and Goldburg showed that the application of an off-resonance irradiation by $\Delta_{LG} = \frac{\nu_1}{\sqrt{2}}$ induces an effective field ($\nu_{eff} = \sqrt{\nu_1^2 + \Delta_{LG}^2}$) inclined at the magic-angle, $\theta_m = \arctan(\sqrt{2}) = \arctan(\frac{\nu_1}{\Delta_{LG}})$, with respect to the static magnetic field, B_0. This effective field is perpendicular to a tilted rotating frame-$\tilde{z}$ (or toggling frame), resulting in an efficient ^{1}H homonuclear decoupling. By applying LG irradiation (perturbation) the spins precess around the effective field or magic-angle axis (1, 1, 1), thus cancelling the dipolar Hamiltonian to first order, over a period of $\tau_{LG} = \sqrt{\frac{2}{3\langle\nu_1\rangle^2}}$, i.e., the time to complete a 2π rotation around the tilted field. By simultaneously switching the RF phase and carrier frequency, between opposite signals, ($\nu_{eff} = \pm\Delta_{LG}/\cos\theta_m$) the effective field direction may be inverted, producing a LG-type experiment symmetric by reflection, named FS-LG. This experiment improves the dipolar truncation to second order by eliminating all even-order terms [23]. To first order, the homonuclear dipolar couplings are averaged out, whereas shielding (isotropic and anisotropic parts) is scaled by a theoretical factor of $1/\sqrt{3}$. This technique requires high-switching speed (<1 μs) of the four-phase modulator (4-PM) to rapidly change the offset frequency ($\pm\Delta_{LG}$).

2. Experimental section

2.1. Synthesis

Microporous aluminophosphate IST-1 was synthesized according to [24].

2.2. Infrared spectroscopy

FT-IR spectra were measured using KBr pellets (Aldrich, 99%+, FT-IR grade) on a Matson 7000 FT-IR spectrometer.

2.3. Solid-State NMR

^{1}H, ^{13}C, ^{31}P and ^{27}Al NMR spectra were recorded on a Bruker Avance 400 (9.4 T) spectrometer (DSX model) at, respectively, 400.1, 100.6, 161.9, and 104.3 MHz, using a 4 mm double-bearing probe. To reduce RF inhomogeneity, the sample was restricted to the center of the 4-mm ZrO_2 rotor. 2D FS-LG measurements were performed using a 3 μs ^{1}H 90° pulse. The ^{1}H RF field strength was set to ca. 83 and 100 kHz for, respectively, FS-LG and TPPM decoupling. The phase switching between each Lee–Goldburg (LG) pulse was optimized by monitoring the multiplet-fine structure of adamantane. The optimization of the FS-LG decoupling was performed by acquiring multiple 2D experiments on natural abundance alanine using different power values and checking the resolution in F1. The phase modulation angle for the TPPM decoupling was set to 15.0°, giving a pulse length of 4.4 μs when optimized directly on the IST-1 sample.

Ramped-amplitude cross-polarization (RAMP-CP) [25] was used in the ^{1}H channel to transfer magnetization from ^{1}H to ^{13}C/^{31}P/^{27}Al. The ^{1}H RF field was ramped from 100 to 50% (from 100 to 50 kHz for ^{13}C and ^{31}P, and 50–25 kHz for ^{27}Al), while the X RF field was set to 66, 50, and 12 kHz for ^{13}C, ^{31}P, and ^{27}Al, respectively.

Chemical shifts are quoted in ppm from TMS (^{1}H and ^{13}C), $[Al(H_2O)_6]^{3+}$ (^{27}Al), and 85% H_3PO_4 (^{31}P).

2.3.1. 2D ^{1}H{FS-LG}–X (X = ^{1}H, ^{13}C, ^{31}P, and ^{27}Al) HOMCOR/HETCOR spectra

Before each LG pulse, the frequency offset was alternated between $+\Delta_{LG}$ and $-\Delta_{LG}$ (or $\pm\nu_1/\sqrt{2}$) corresponding to $+58925 + \nu_{lg}$ and $-58925 + \nu_{lg}$ Hz. Best results were obtained using asymmetric offsets during the FS-LG decoupling of about $\nu_{lg} = \pm$ 4–6 kHz [26]. This value is added to the above frequency jumps and is optimized to move the axial artifact out of the spectrum and avoid spectral truncation along F1.

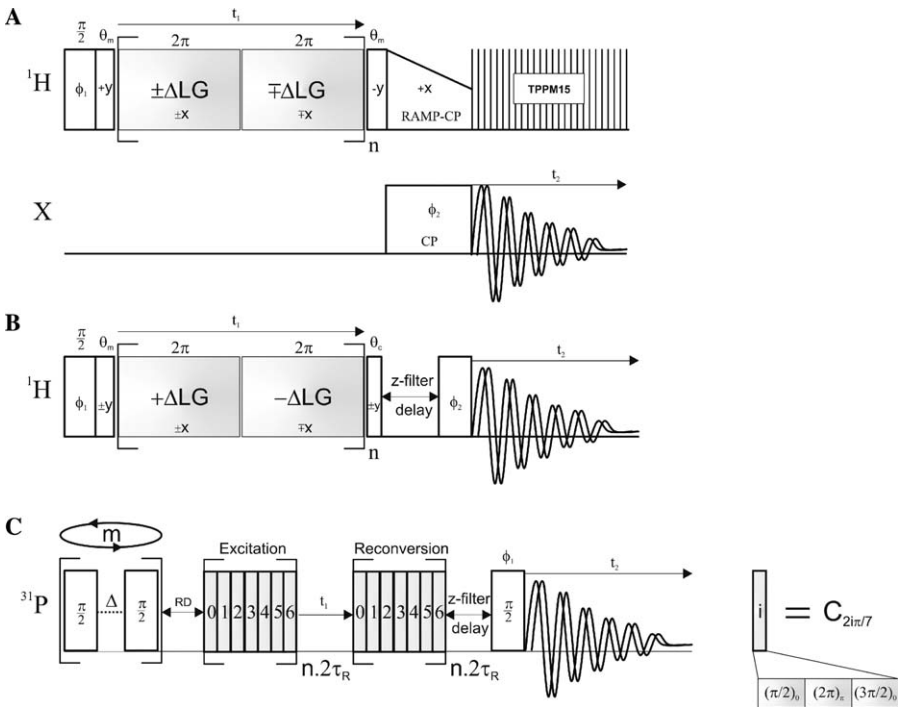

Fig. 1. Pulse sequences used for 2D (A) ^{1}H–X CP HETCOR with RAMP-CP, (B) ^{1}H{FS-LG}–^{1}H HOMCOR, and (C) ^{31}P DQ-SQ correlation sequences (POSTC7 [29]). θ_m is the (magic) angle between the static magnetic field (B_0) and the effective magnetic field (B_{eff}). θ_c is the complementary angle, $\theta_c = \pi/2 - \theta_m$. The nested phase cycling used in the (A and B) pulse schemes is $\phi_1 = +y\ -y$; $\phi_2 = +x\ +x\ -x\ -x\ +y\ +y\ -y\ -y$ and $\phi_{rec} = 0\ 2\ 2\ 0\ 1\ 3\ 3\ 1$. For the POSTC7 sequence (C), the values of m, n, RD and z-filter (z) are depicted in the figure captions. The 90° detection pulse phase cycling is: $\phi_1 = 0\ 0\ 0\ 0\ 1\ 1\ 1\ 1\ 2\ 2\ 2\ 2\ 3\ 3\ 3\ 3$ and the receiver phases are: $\phi_{rec} = 2\ 0\ 2\ 0\ 3\ 1\ 3\ 1\ 0\ 2\ 0\ 2\ 1\ 3\ 1\ 3$ for the cosine part, and $\phi_{rec} = 0\ 2\ 0\ 2\ 1\ 3\ 1\ 3\ 2\ 0\ 2\ 0\ 3\ 1\ 3\ 1$ for the sine part.

2D ^{1}H{FS-LG}–X dipolar HETCOR and 2D ^{1}H{FS-LG}–^{1}H dipolar HOMCOR experiments were performed using the pulse sequences (and phase cycling scheme) depicted in Figs. 1A and B, respectively [18]. 2D ^{1}H{FS-LG}–^{1}H dipolar HOMCOR experiments were acquired using a z-filter (mixing time) delay with null time to avoid spin diffusion. The LG pulse length (τ_{LG}) was set to 9.8 μs and, thus, one FS-LG unit equals two successive τ_{LG} units. Quadrature detection in t_1 was achieved using the States-TPPI method [27]. For the FS-LG HOMCOR/HETCOR schemes, the ^{1}H chemical shift scale and the scaling factors λ were determined by comparing the 1D ^{1}H spectra recorded under fast MAS (30 kHz) and under the FS-LG homonuclear decoupling sequence determined by direct comparison with the scaled ^{1}H{FS-LG}–^{1}H HOMCOR spectra [18,28]. Scaling factors of 0.56–0.58 were obtained for all spectra, within the range of the theoretical value. Specific experimental conditions of each spectrum are given in the figure captions.

2.3.2. 2D ^{31}P–^{31}P DQ HOMCOR

The pulse sequence employed for the ^{31}P–^{31}P DQ measurements is shown in Fig. 1C. Prior to the relaxation delay, a saturation comb of 90° pulses was applied. The POSTC7 sequence was chosen to reintroduce the ^{31}P–^{31}P homonuclear dipolar interaction under MAS conditions and to achieve an efficient broad band excitation and reconversion of the DQ coherences [29]. The 90° pulse was set to 3.6 μs and the phases were adjusted by using a combination between the digital phase shifter ($n \times 7 \times \frac{2\pi}{7}$ phase increments intercalated by a phase preset of 0.3 μs) and the four-phase modulator (alternating between $+x$ and $-x$ according to the pulse sequence in Fig. 1). Further details on the experimental conditions are given in the figure captions. After t_1 evolution, the DQ coherences were reconverted using the excitation pulse sequence, with an overall constant phase shift of $\pi/2$ to achieve time reversal. For quadrature detection during t_1, the States mode was employed [27]. No ^{1}H decoupling was applied during acquisition.

3. Results and discussion

3.1. Structure description

The structure of IST-1 (Figs. 2 and 3) was refined from high-resolution synchrotron powder X-ray diffraction data in the non-centrosymmetric space group $Pca2_1$, in tandem with solid-state NMR [22]. Here, we concentrate our attention on the following structural features of IST-1: (i) one methylamine species probably protonated [MA$^+$, C(2)–N(2)], resides in the channels and is hydrogen-bonded to three framework oxygen atoms; (ii) a second methylamine molecule [MA, C(1)–N(1)] bonds directly to a framework Al atom, a relatively uncommon structural feature among aluminophosphates.

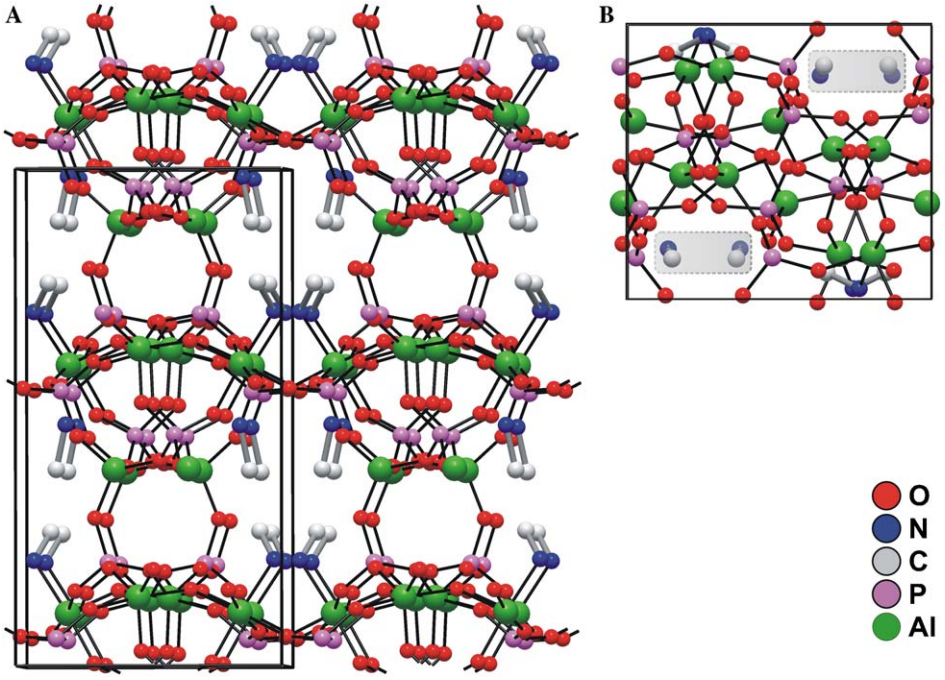

Fig. 2. (A) Crystal packing viewed in perspective along the *a*-axis. (B) Unit cell contents viewed along the *c*-axis depicting the location of the extra-framework MA [C(2)–N(2)] species inside the IST-1 pores.

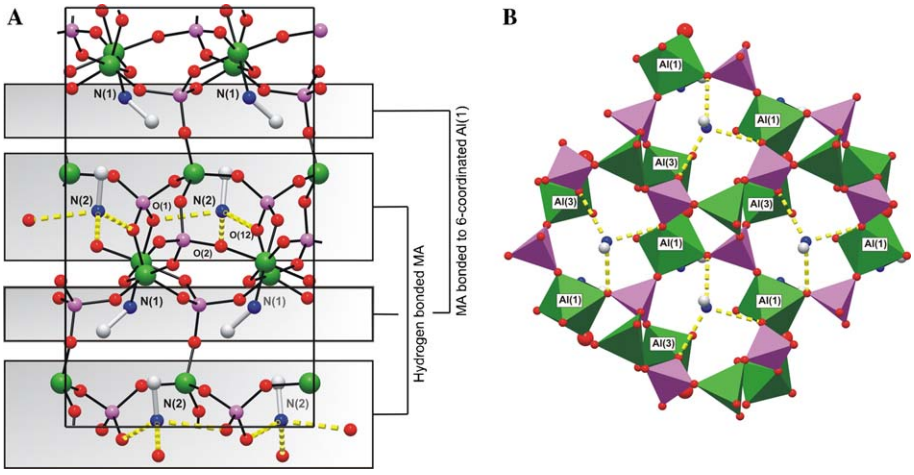

Fig. 3. (A) Schematic representation, viewed down the *b*-axis, showing the MA, [N(1)–C(1)], species coordinated to Al(1), and the protonated MA^+ species (residing in the channels, hydrogen bonded to three framework O-atoms [O(1), O(2) and O(12)]). (B) Polyhedral representation of the structure of IST-1 viewed down the *c*-axis.

3.2. Spectral analysis

3.2.1. ^1H NMR

The $^1H\{FS\text{-}LG\}$–^1H HOMCOR spectrum of IST-1 (Fig. 4) exhibits four well-resolved resonances at ca. 1.2, 2.4, 3.9 and 7.8 ppm, attributed to the Al-OH, CH_3, NH_2 (MA) and NH_3^+ (MA^+) species, respectively. Usually, protonated amines resonate at high frequency, typically 7.0–9.0 ppm, depending on the nature of H-bonding network present [18,30,31]. The previous structural study did not provide definitive proof for the presence of MA^+ cations in IST-1 [22]. However, the resonance at ca. 7.8 ppm (Fig. 4) is clearly attributed to ^+N–H···O^- interactions. The large N–Al bond length [2.10(1) Å] and, thus, weak chemical bond helps understanding why the NH_2 resonance is much shifted to low frequency relatively to NH_3^+ resonance (3.9 and 7.8 ppm). The spectrum also displays a peak at 1.2 ppm, tentatively assigned to bridging O–H [Al(1)–O*H*–Al(3)] groups, which resonate at 0.8–1.5 ppm [30,31], or non-acidic terminal Al–OH groups in AlPOs [32].

In accord with the NMR evidence, the FT-IR spectrum shows group frequencies typical of protonated amines: (i) stretching vibrations, $\nu(NH_3^+) = 3115\ cm^{-1}$; (ii) asymmetric and symmetric bending vibrations, $\delta_{as}(NH_3^+) = 1610$ and $\delta_s(NH_3^+) = 1532\ cm^{-1}$; (iii) wagging vibrations,

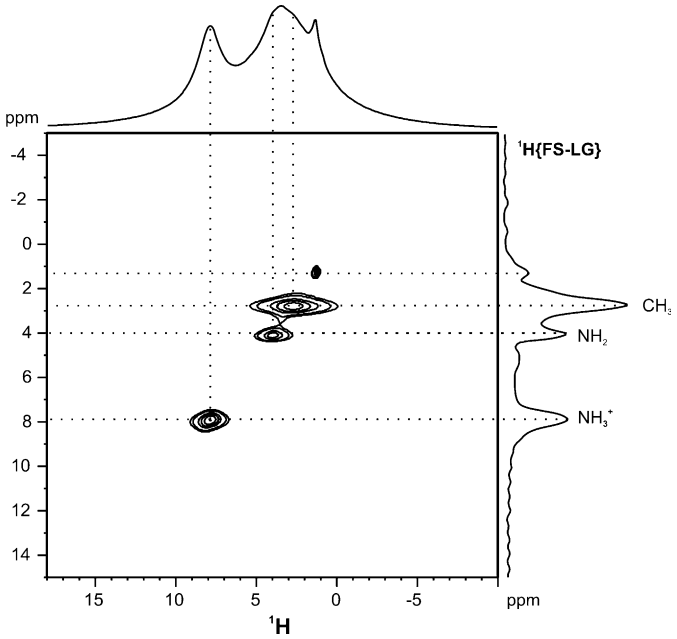

Fig. 4. 2D ^{1}H{FS-LG}–^{1}H HOMCOR spectrum of IST-1. A total of 200 t_1 increments with eight transients each were collected. F1 increments were synchronized with an integer number of FS-LG units ($n \cdot 2 \cdot \tau_{LG}$) with $n = 3$. The value of ν_{lg} was ±3000 Hz and the recycle delay 3 s.

$\omega(NH_3^+) = 730$ and 710 cm^{-1}; and (iv) the typical torsional vibrations of NH_3^+ at 536 and 515 cm^{-1}.

3.2.2. ^{13}C NMR

The interpretation of the ^{1}H–X (X = ^{13}C, ^{31}P, and ^{27}Al) HETCOR spectra is assisted by considering the interatomic separations obtained from the synchrotron powder X-ray diffraction structure [23]. Because no neutron diffraction data were collected, reliable H···X distances are not available. Instead, distances between X and the atom to which a given proton is linked will be considered.

The 2D ^{1}H{FS-LG}–^{13}C CP HETCOR spectrum recorded with a contact time (CT) of 2000 μs [Fig. 5A] is uninformative because all peaks are correlated. However, the spectrum recorded with CT = 200 μs [Fig. 5B] clearly shows that (i) the ^{1}H resonance at ca. 2.4 ppm is attributed to the CH_3 groups, and (ii) the ^{13}C resonance at ca. 24.5 ppm is unambiguously assigned to the MA^+ carbon [C(2)], because a unique cross-peak is observed between it and the MA^+ proton peak (ca. 7.8 ppm). The latter conclusion is in contrast with the tentative assignment of the ^{13}C resonances based on computational models [22].

An outstanding feature of the F2 (^{13}C axis) projections of the spectra in Fig. 5 is the presence of asymmetric dou-

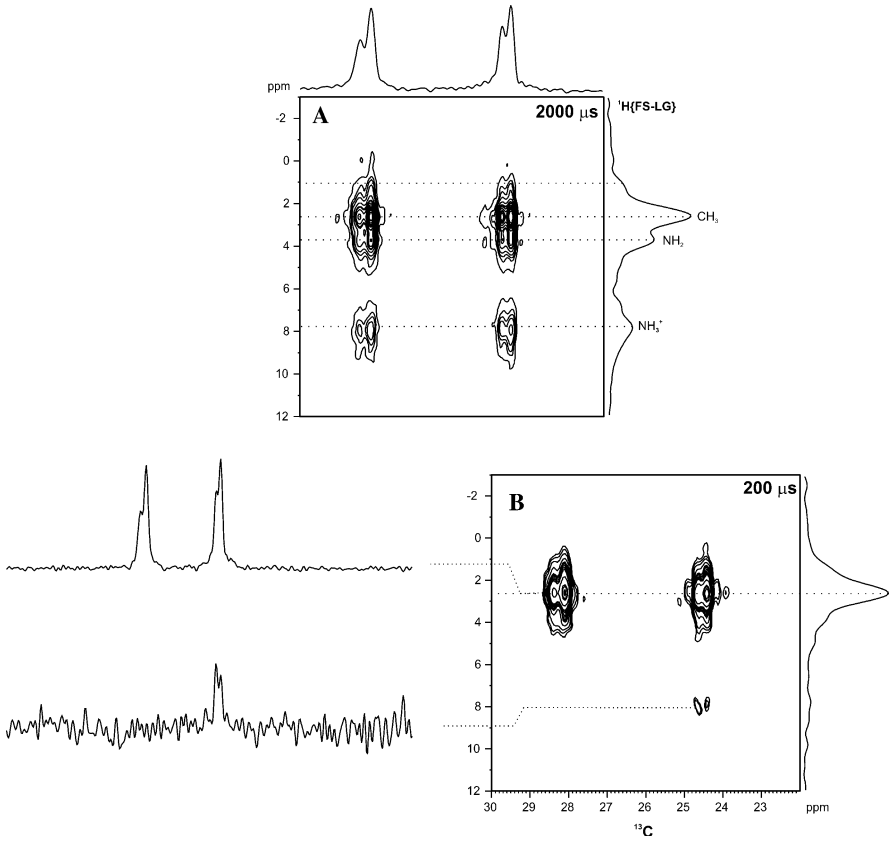

Fig. 5. 2D ^{1}H{FS-LG}–^{13}C CP HETCOR NMR spectra of IST-1 recorded with (A) CT = 2000 and (B) CT = 200 μs. 90 t_1 increments with 164 transients each were collected. The F1 increments were synchronized with an integer number of FS-LG units ($n \cdot (2 \cdot \tau_{LG})$) with $n = 3$. The recycle delay was 3 s and the value of ν_{lg} was −5000 Hz. The F2 slices of selected cross-peaks are depicted on the left.

blets centred at ca. 24.5 and 28.2 ppm, which may be attributed to the: (i) presence of four non-equivalent MA species, or (ii) unaveraged ^{13}C–^{14}N dipolar coupling involving the quadrupolar nucleus ^{14}N [33,34]. The latter usually yields asymmetric doublets with intensities in a 2:1 ratio, which is clearly observed in the ^{1}H–^{13}C CP-MAS spectra shown in Fig. 6. However, this splitting is usually observed at relatively low B_0 fields and, to the best of our knowledge, has not yet been reported at 9.4 T.

The splitting observed in Fig. 6 arises because the ^{14}N spin states are not purely Zeeman in nature ($|\psi_k\rangle$, with $k = -1, 0, +1$). In a ^{13}C–^{14}N coupled spin pair, the quantization axis of ^{14}N spin is not strictly along the external magnetic field (B_0) since the quadrupolar interaction of ^{14}N has, in many cases, a magnitude comparable to that of the Zeeman interaction. Several systems have been investigated where the first-order perturbation accounts for the effect of residual dipolar coupling to quadrupolar nuclei in solid-state NMR spectra of spin-1/2 nuclei [20,35–41].

Olivieri and Harris [20,39,40] derived first- and second-order effects on the ^{13}C resonance, the latter showing a dependence of the ^{13}C splitting, ($^{(2)}\Delta\nu_K$) on parameters such as the C–N distance, static magnetic field and quadrupolar constant:

$$^{(2)}\Delta\nu_K = \frac{D^{IS}C_Q}{\nu_S} \times \frac{3S(S+1) - 9k^2}{20S(2S-1)} \times 3\cos^2\beta - 1 + \eta\sin^2\beta\cos 2\alpha, \quad (1)$$

where β and α are the polar angles specifying the orientation of the I–S internuclear vector with respect to the EFG tensor, and ν_S is the S (^{14}N) spins Larmor frequency. Eq. (1) is only applicable if certain assumptions hold [20].

Eq. (1) shows that the peak positions depend on k^2 and, thus, the $|\psi_{\pm k}\rangle$ state (i.e., $|\psi_{\pm 1}\rangle$ for the ^{14}N nucleus) produces the same shift, since the signal does not influence the eigenstates. The result is the superposition of the $|\psi_{+1}\rangle$ and $|\psi_{-1}\rangle$ states at the same frequency and $|\psi_0\rangle$ at a different frequency, thus yielding the theoretical 2:1 ratio [20,39,40]. Eq. (1) further shows an inverse dependence of the ^{13}C splitting with the S spins Larmor frequency, in agreement with our results (Fig. 6A). Increasing the magnetic field from 9.4 to 11.7 T reduces the splitting, indicating that the ^{14}N second-order quadrupolar effects influence the ^{13}C–^{14}N dipolar interaction. In principle, the splittings observed for the two resonances, may support the assignment made on the basis of the 2D $^{1}H\{FS\text{-}LG\}$–^{13}C HETCOR spectra (Fig. 5). Olivieri et al. [40] reported a nearly

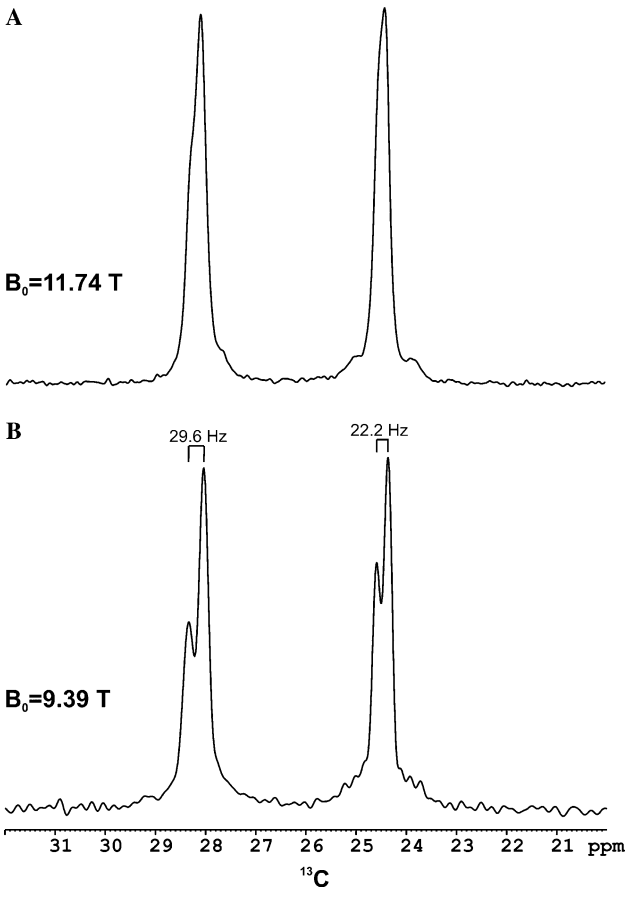

Fig. 6. Ramped ^{1}H–^{13}C CP-MAS spectra showing the effect of the Zeeman field (B_0) on the asymmetric doublet pattern. Spectra were acquired at (A) 11.74 T and (B) 9.39 T. The heteronuclear decoupling RF field and the spinning speed used were set to $\upsilon_1 = 100$ kHz and $\upsilon_R = 12$ kHz, respectively. TPPM-15 was used as the heteronuclear decoupling scheme. The magic angle was very carefully adjusted to obtain the best resolution.

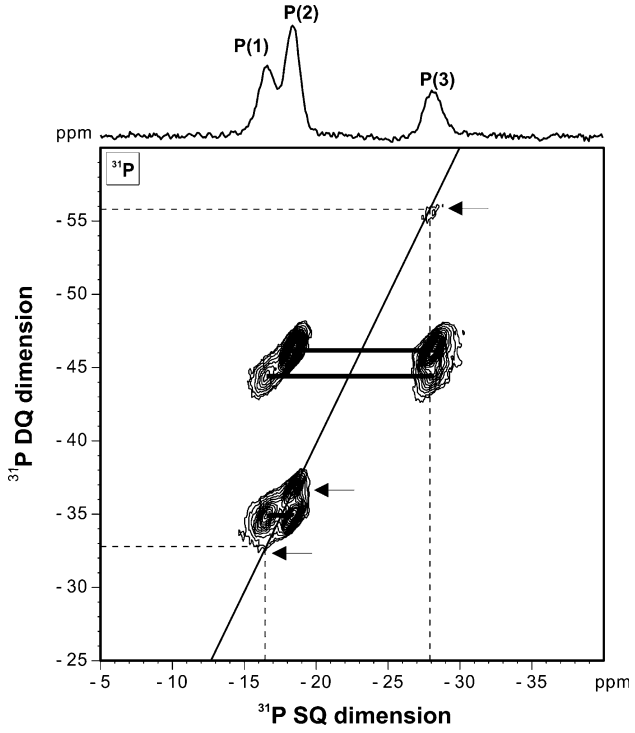

Fig. 7. ^{31}P–^{31}P double-quantum HOMCOR spectrum of IST-1. A total of 120 t_1 points synchronized with the rotor period [$(1/\upsilon_R) = 100$ μs] with 16 transients each were collected. The DQ excitation/reconversion times were 1 ms ($n = 5$, see Fig. 1), $m = 10$, RD = 30 s and z (z-filter) = $1/\upsilon_R$. Autocorrelation peaks are depicted with arrows and the 2Q coherences between the three different ^{31}P resonances (cross-peaks) are also indicated [22].

linear relationship between the C–N crystallographic distances and the ^{13}C splittings, i.e, the shorter the C–N distance the larger the splitting value. In IST-1, the C–N distances of the MA (resonance at ca. 28.2 ppm) and MA^+ (ca. 24.5 ppm) species are 1.481 and 1.499 Å, respectively. Since the C–N distances are very similar the quadrupole coupling constants (CQs) of both species probably determine the size of the splittings. However, the CQ's of the ^{14}N nuclei are unknown.

3.2.3. ^{31}P NMR

The 2D ^{31}P–^{31}P double-quantum (DQ) HOMCOR experiment was performed in order to confirm the previous ^{31}P assignment, based upon ^{27}Al–^{31}P HETCOR evidence [22] which, because of the complicated spin dynamics involved in the spin locking and polarization transfer between spin-1/2 quadrupolar nuclei, was only tentative. Moreover, ^{27}Al–^{31}P HETCOR spectroscopy requires a third NMR channel which is not necessary for recording 2D ^{31}P DQ spectra.

Table 1
P···P crystallographic distances in IST-1 structure (Å)

P sites[a]	P(1)	P(2)	P(3)
P(1)	5.65		
P(2)	4.57	5.03	
P(3)	4.90	4.23	5.48

[a] Labeling scheme follows the notation presented in the ^{31}P spectra of Figs. 7 and 8 is in accord with the X-ray structure [22].

Consider the F2 (^{31}P) projection in Fig. 7. The resonances of the three unique P sites of IST-1 have been labeled according to the internuclear P···P distance depicted in Table 1 [22]. The strongest ^{31}P auto-correlation peak (diagonal) is attributed to P(2) because the P(2)···P(2) distance is the shortest one. As expected, the P(3)···P(3) peak is very weak, while the P(1)···P(1) correlation is absent. With this information in hand, the assignment of the cross-peaks is straightforward and it may be confirmed by considering the cross-peak intensities (Fig. 7). Clearly, the strongest cross-peaks are P(2)···P(3) and the faintest P(1)···P(3).

Consider now the 2D $^{1}H\{FS\text{-}LG\}$–^{31}P CP HETCOR spectra in Fig. 8. In accord with the X-ray structure, the less intense cross-peaks are observed between P and H atoms which are further apart: P(2)···N(1) (5.3 Å) and

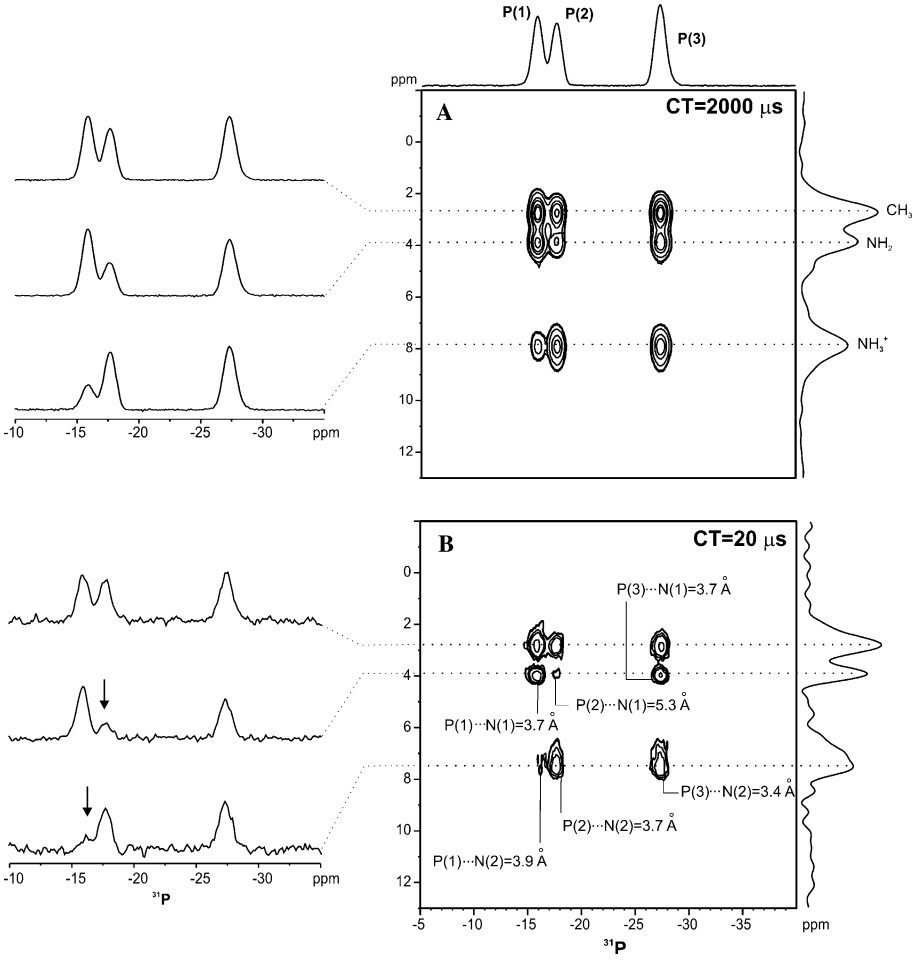

Fig. 8. 2D $^{1}H\{FS\text{-}LG\}$–^{31}P CP HETCOR NMR spectra of IST-1 recorded with (A) CT = 2000 and (B) CT = 20 μs. 90 t_1 increments with 72 transients each were collected. The F1 increments were synchronized with an integer number of FS-LG units ($n \cdot (2 \cdot \tau_{LG})$) with $n = 3$. The recycle delay was 3 s and the value of ν_{lg} employed was −5000 Hz.

P(1)···N(2) (3.9 Å). The spectrum in Fig. 8 supports the assignment of MA and MA^+ species made previously. The distances depicted in Fig. 8B are consistent with the cross-peak intensities observed. For instance, the distance P(2)···N(1) is, by far, the longest (5.3 Å). Accordingly, the faint cross-peak correlating P(2) and the $–NH_2$ [HN(1)–Al] groups is correctly labeled in Fig. 8, allowing the assignment of the C(1)–N(1) to the MA residues resonating at ca. 3.9 ppm ($–NH_2$). The ^{1}H resonances of C(2)–N(2) may, thus, be assigned to the MA^+ species resonating at ca. 7.8 ppm ($–NH_3^+$). The P(1)···N(2) cross-peak is much less intense than the P(2), P(3)···N(2) cross-peaks, presumably because the P(1)···N(2) distance is the longest (respectively, 3.9 and 3.7 and 3.4 Å).

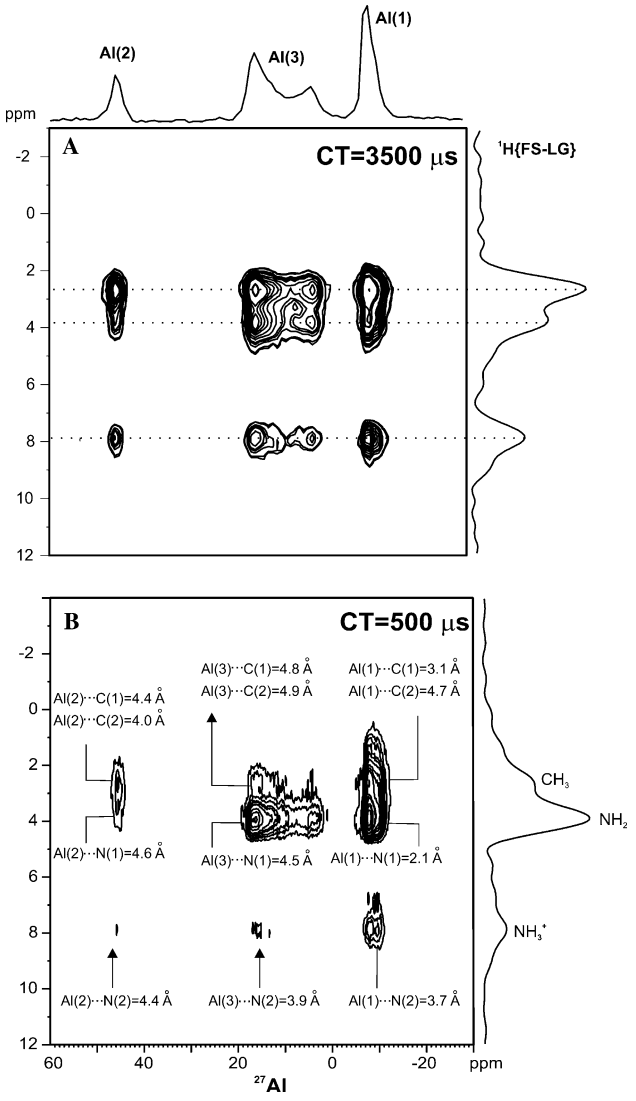

Fig. 9. 2D ^{1}H{FS-LG}–^{27}Al CP HETCOR NMR spectra of IST-1 recorded with (A) CT = 3500 and (B) CT = 500 μs. 128 t_1 increments with 8 transients each were collected for (A) and 128 t_1 increments with 80 transients each were collected for (B). The F1 increments were synchronized with an integer number of FS-LG units ($n \cdot (2 \cdot \tau_{LG})$) with $n = 3$. The recycle delay was 3 s and the value of ν_{lg} was −5000 Hz.

3.2.4. ^{27}Al NMR

The ^{1}H{FS-LG}–^{27}Al CP HETCOR spectra of Fig. 9, confirm that five-coordinated Al is the furthest from the CH_3 groups [$d_{Al(3)–C(1)} = 4.8$ Å, $d_{Al(3)–C(2)} = 4.9$ Å]. The six-coordinated Al [N(1)···Al(1)] still gives the strongest cross-peak at short CT, as expected. The peak tail at ca. 1.2 ppm in F1 [Fig. 9B] may be due to the O(13)–H protons bridging the five- and six-coordinated Al sites. This is further supported by the presence of a strong and narrow O–H stretching FT-IR band at ca. 3512 cm^{-1}.

The $–NH_2$ proton resonance, is clearly observed in the ^{1}H{FS-LG}–^{27}Al HETCOR spectra at low CT, while the other resonances become faint. This is because five- and six-coordinated Al [Al(3) and Al(1), respectively] are relatively close to the MA residues coordinated to Al(1) [consider the Al···N distances in Fig. 9B]. The extraction of more information from these spectra is prone to error, due to the complicated spin dynamics involving quadrupolar nuclei during spin locking [42,43], which can influence the peak intensity by quadrupolar relaxation effects.

4. Conclusion

The local ^{13}C, ^{31}P, ^{27}Al and ^{1}H environments in IST-1 have been studied by two-dimensional high-resolution NMR techniques such as ^{1}H{FS-LG}–^{1}H HOMCOR, 2D ^{1}H{FS-LG}–X HETCOR and ^{31}P DQ-SQ correlation techniques (X = ^{31}P, ^{13}C, and ^{27}Al).

High-resolution ^{1}H NMR techniques employing FS-LG homonuclear decoupling, used in tandem with X-ray crystallographic evidence, have been shown to be useful tools to investigate the structure of the microporous aluminophosphate IST-1. In this study, we have:

- Proven the existence of protonated amine in the IST-1 pores (MA^+ residues);
- Unambiguously assigned the resonances of methylamine MA species, covalently bonded to a framework Al, and MA^+ residues inside the pores, by combining ^{1}H{FS-LG}-^{1}H HOMCOR and ^{1}H{FS-LG}–^{13}C/^{31}P/^{27}Al HETCOR techniques;
- Assigned the ^{31}P crystallographic environments by combining ^{31}P–^{31}P DQ-SQ and ^{1}H{FS-LG]–^{31}P HETCOR experiments.

Acknowledgments

We are grateful to FEDER, POCTI (Portugal), Portuguese Foundation for Science and Technology (FCT) and NoE FAME for their general financial support and the Ph.D. research Grant No. SFRH/BD/13858/2003 (to L.M.). We thank Dr. Hans Förster, Solids Applications at *Bruker-Biospin*, Karlsruhe, for technical support. We also thank Prof. F. Ribeiro from *Instituto Superior Técnico*, Lisbon, for sending us the IST-1 material.

References

[1] M. Lee, W.I. Goldburg, Nuclear-Magnetic-Resonance line narrowing by a rotating rf field, Phys. Rev. 140 (1965) 1261.

[2] J.S. Waugh, L.M. Huber, U. Haeberlen, Approach to high-resolution NMR in solids, Phys. Rev. Lett. 20 (1968) 180–182.

[3] W.K. Rhim, D.D. Elleman, R.W. Vaughan, Enhanced resolution for solid state NMR, J. Chem. Phys. 59 (1973) 3740–3749.

[4] P. Mansfield, Symmetrized pulse sequences in high resolution NMR in solids, J. Phys. C: Solid State Phys. 4 (1971) 1444–1452.

[5] D.P. Burum, W.K. Rhim, Analysis of multiple pulse NMR in solids, J. Chem. Phys. 71 (1979) 944–956.

[6] D.P. Burum, M. Linder, R.R. Ernst, Low-power multipulse line narrowing in solid-state NMR, J. Magn. Reson. 44 (1981) 173–188.

[7] K. Takegoshi, C.A. McDowell, A "magic echo" pulse sequence for the high-resolution NMR spectra of abundant spins in solids, J. Phys. Chem. 116 (1985) 100–104.

[8] M. Hohwy, P.V. Bower, H.J. Jackobsen, N.C. Nielsen, A high-order and broadband CRAMPS experiment using z-rotational decoupling, J. Chem. Phys. 97 (1997) 297–303.

[9] D. Sakellariou, A. Lesage, P. Hodgkinson, L. Emsley, Homonuclear dipolar decoupling in solid-state NMR using continuous phase modulation, Chem. Phys. Lett. 319 (2000) 253–260.

[10] A. Bielecki, A.C. Kolbert, M.H. Levitt, Frequency-switched pulse sequences: homonuclear decoupling and dilute spin NMR in solids, Chem. Phys. Lett. 155 (1989) 341–346.

[11] M. Hohwy, N.C. Nielsen, Elimination of high order terms in multiple pulse nuclear magnetic resonance spectroscopy: application to homonuclear decoupling in solids, J. Chem. Phys. 106 (1997) 7571–7586.

[12] E. Vinogradov, P.K. Madhu, S. Vega, High-resolution proton solid-state NMR spectroscopy by phase-modulated Lee-Goldburg experiment, Chem. Phys. Lett. 314 (1999) 443–450.

[13] E. Vinogradov, P.K. Madhu, S. Vega, A bimodal Floquet analysis of phase modulated Lee-Goldburg high resolution proton magic angle spinning NMR experiments, Chem. Phys. Lett. 329 (2000) 207–214.

[14] E. Vinogradov, P.K. Madhu, S. Vega, Phase modulated Lee-Goldburg magic angle spinning proton nuclear magnetic resonance experiments in the solid state: a bimodal floquet theoretical treatment, J. Chem. Phys. 115 (2001) 8983–9000.

[15] E. Vinogradov, P.K. Madhu, S. Vega, Proton spectroscopy in solid state nuclear magnetic resonance with windowed phase modulated Lee-Goldburg decoupling sequences, Chem. Phys. Lett. 354 (2002) 193–202.

[16] L.M. Ryan, R.E. Taylor, A.J. Paff, B.C. Gerstein, An experimental study of resolution of proton chemical shifts in solids: combined multiple pulse NMR and magic-angle spinning, J. Chem. Phys. 72 (1980) 508–515.

[17] B.C. Gerstein, R.G. Pembleton, R.C. Wilson, L.M. Ryan, High resolution NMR in randomly oriented solids with homonuclear dipolar broadening: combined multiple pulse NMR and magic angle spinning, J. Chem. Phys. 66 (1977) 361–362.

[18] B.J. van Rossum, H. Forster, H.J.M. deGroot, High-field and high-speed CP-MAS C-13 NMR heteronuclear dipolar-correlation spectroscopy of solids with frequency-switched Lee-Goldburg homonuclear decoupling, J. Magn. Reson. 124 (1997) 516–519.

[19] S.T. Wilson, B.M. Lok, C.A. Messina, T.R. Cannan, E.M. Flanigen, J. Am. Chem. Soc. 104 (1982) 1146.

[20] W.T.A. Harrison, Templated inorganic networks: recent developments, Curr. Opin. Solid State Mater. Sci. 6 (2002) 407–413.

[21] K. Wang, J. Yu, P. Miao, Y. Song, J. Li, Z. Shi, R. Xu, A new layered aluminophosphate [C4H12N2][Al2P2O8(OH)2] templated by piperazine, J. Mater. Chem. 11 (2001) 1898–1902.

[22] J.L. Jordá, L.B. McCusker, C. Baerlocher, C.M. Morais, J. Rocha, C. Fernandez, C. Borges, J.P. Lourenço, M.F. Ribeiro, Z. Gabelica, Structure analysis of the novel microporous aluminophosphate IST-1 using synchrotron powder diffraction data and HETCOR MAS NMR, Microporous Mesoporous Mater. 65 (2003) 43–57.

[23] W.K. Rhim, D.D. Elleman, Analysis of multiple pulse NMR in solids, J. Am. Chem. Phys. 59 (1973) 3740–3749.

[24] A. Fernandes, M.F. Ribeiro, C. Borges, J.P. Lourenço, J. Rocha, Z. Gabelica, Two new aluminophosphates, IST-1 and IST-2: first examples of a dual templating role of water and methylamine in generating microporous structures, Microporous Mesoporous Mater. 90 (2006) 112–128.

[25] G. Metz, X.L. Wu, S.O. Smith, Ramped-amplitude cross-polarization in magic-angle-spinning NMR, J. Magn. Reson. Series A 110 (1994) 219–227.

[26] A. Lesage, D. Sakellariou, S. Steuernagel, L. Emsley, Carbon-proton chemical shift correlation in solid-state NMR by through-bond multiple-quantum spectroscopy, J. Am. Chem. Soc. 120 (1998) 13194–13201.

[27] D.J. States, R.A. Haberkorn, D.J. Ruben, A two-dimensional nuclear overhauser experiment with pure absorption phase in four quadrants, J. Magn. Reson. 48 (1982) 286–292.

[28] B.J. van Rossum, F. Castellani, K. Rehbein, J. Pauli, H. Oschkinat, Assignment of the nonexchanging protons of the alpha-spectrin SH3 domain by two- and three-dimensional H-1-C-13 solid-state magic-angle spinning NMR and comparison of solution and solid-state proton chemical shifts, Chembiochem 2 (2001) 906–914.

[29] M. Hohwy, H.J. Jakobsen, M. Eden, M.H. Levitt, N.C. Nielsen, Broadband dipolar recoupling in the nuclear magnetic resonance of rotating solids: a compensated C7 pulse sequence, J. Chem. Phys. 108 (1998) 2686.

[30] M. Hunger, S. Ernst, S. Steuernagel, J. Weitkamp, High-field ^{1}H MAS NMR investigations of acidic and non-acidic hydroxyl groups in zeolites H-Beta, H-ZSM-5, H-ZSM-58 and H-MCM-22, Microporous Mater. 6 (1996) 349–353.

[31] K. Maeda, A. Tuel, C. Baerlocher, Synthesis and characterization of a new layered aluminophosphate templated with 1,3-diaminopropane: $[H_3N(CH_2)_3NH_3]_{0.5}[AlPO_4(OH)(OH_2)].H_2O$, J. Chem. Soc., Dalton Trans. (2000) 2457–2462.

[32] M.H. Zahedi-Niaki, S.M. Javaid Zaidi, S. Kaliaguine, Acid properties of titanium aluminophosphate molecular sieves, Microporous Mesoporous Mater. 32 (1999) 251–255.

[33] S.J. Opella, M.H. Frey, Detection of individual carbon resonances in solid proteins, J. Am. Chem. Soc. 101 (1979) 5856–5857.

[34] C.A. McDowell, in: D.M. Grant, R.K. Harris (Eds.), Encyclopedia of Nuclear Magnetic Resonance, Vol. 5, 1996, pp. 2901–2908.

[35] K. Eichele, D. Lumsden, R.E. Wasylishen, Nitrogen-14 coupled dipolar-chemical shift 13C NMR spectra of the amide fragment of peptidesin the solid state, J. Phys. Chem. 97 (1993) 8909–8916.

[36] Z. Gan, D.M. Grant, Molecular and structural information from variable-angle spinning NMR dipolar spectra of ^{13}C–^{14}N systems, J. Magn. Reson. 90 (1990) 522–534.

[37] J.G. Hexem, M.H. Frey, S.J. Opella, Influence of ^{14}N on ^{13}C NMR spectra of solids, J. Am. Chem. Soc. 103 (1981) 224–226.

[38] A. Naito, S. Ganapathy, C.A. McDowell, ^{14}N quadrupole effects in CP-MAS ^{13}C NMR spectra of organic compounds in the solid state, J. Magn. Reson. 48 (1982) 367–381.

[39] A.C. Olivieri, Quadrupolar effects in the CP-MAS NMR spectra of spin-1/2 nuclei, J. Magn. Reson. 81 (1989) 201–205.

[40] A.C. Olivieri, L. Frydman, L.E. Diaz, A simple approach for relating molecular and structural information to the dipolar coupling ^{13}C–^{14}N in CPMAS NMR, J. Magn. Reson. 75 (1987) 50–62.

[41] C.E. Hughes, R. Pratima, T. Karlsson, M.H. Levitt, Double-quantum solid-state NMR of ^{13}C spin pairs coupled to ^{14}N, J. Magn. Reson. 159 (2002) 25–35.

[42] S.E. Ashbrook, S. Wimperis, Spin-locking of half-integer quadrupolar nuclei in nuclear magnetic resonance of solids: creation and evolution of coherences, J. Chem. Phys. 120 (2004) 2719–2731.

[43] A.J. Vega, Mas NMR spin locking of half-integer quadrupolar nuclei, J. Magn. Reson. 96 (1992) 50–68.